ANNALS OF GEOPHYSICS, 66, 5, DM526, 2023; doi:10.4401/ag-8982
OPEN ACCESS

The March 2023 UAS-based high-resolution Digital Surface Model and orthomosaic of the NE flank of Stromboli volcano (Sicily, Italy)

Luca Nannipieri[1], Andrea Bevilacqua[1], Federico Di Traglia[2], Massimiliano Favalli[1] and Alessandro Fornaciai[*,1]

(1) Istituto Nazionale di Geofisica e Vulcanologia, Sezione di Pisa, Italy.
(2) Istituto Nazionale di Geofisica e Vulcanologia, Sezione di Napoli, Osservatorio Vesuviano, Italy

Article history: received May 25, 2023; accepted November 14, 2023

Abstract

Stromboli is a volcanic island in a persistent state of activity, located in the Tyrrhenian Sea off the northern coast of Sicily. During the night of 25 and 26 May 2022, a massive human-caused wildfire destroyed most of the vegetation cover on the NE flank of the island, just above the main village. On 12 August 2022, a particularly heavy rainfall event remobilized the loose volcaniclastic deposits that covered the burned volcanic flank, no longer protected by the vegetation. This event triggered several debris flows that were channeled by the roads and flooded several streets and buildings, causing severe damage to the village. In late-March 2023, just before the large spring vegetation growth, we conducted an Unmanned Aerial System (UAS) photogrammetric campaign over a sector of the NE flank of Stromboli Island, to acquire data on an area massively affected by the wildfire first and by the debris flows later. Here we present and share with the scientific community and civil authorities the results of this UAS campaign, which consists of a 1.4 km^2 wide 10 cm-resolution Digital Surface Model (DSM) and 1.6 cm-resolution orthomosaic. These data clearly show the dramatic consequences of the 2022 tragic events at Stromboli. We also produced an elevation difference map by comparing the 2023 DSM here generated and the 2012 LiDAR DEM to provide a first overview of the thickness of the deposits that were removed from the Stromboli NE flank.

Keywords: Stromboli; Unmanned Aerial System; Orthophotos; Digital Surface Model; Wildfire; Volcaniclastic debris flow

1. Introduction

The steep flanks of active volcanic islands stand in a fragile equilibrium. Large volumes of incoherent products are periodically accumulated on steep slopes where they can be easily remobilized by intense rainfall events [Thouret *et al.*, 2020]. The growth of vegetation over unconsolidated volcanic deposits plays a crucial role in preventing their remobilization and, in general, in stabilizing steep slopes. Severe wildfires, burning the vegetation cover, re-expose the volcaniclastic loose deposits to the precipitation and, consequently, to an increase in rain

splash erosion [Providoli *et al.*, 2002; Areu-Rangel *et al.*, 2020]. Moreover, the passage of fires decreases the water infiltration capacity and that, as a result, increases surface runoff [Giovannini, 1994, Giovannini *et al.*, 2001; Ortíz-Rodríguez *et al.*, 2019]. Finally, once the vegetation is dead, the dead roots no longer anchor the loose deposits. It follows that when a large wildfire impacts on steep volcanic flanks, the resulting hydrogeological alterations [Wondzell and King, 2003], particularly in the months and years immediately after the fire event, strongly increase the likelihood of floods and debris flows [e.g. Bisson *et al.*, 2005].

Stromboli is a 924 m-high volcanic island, located in the Tyrrhenian Sea off the northern coast of Sicily (Figure 1), in perennial state of activity. Island landscapes resulted from the interaction between volcanic activity, geomorphological evolution, and traditional land management [Turchi *et al.*, 2022]. During violent explosions, incandescent ejecta often reach the vegetation causing wildfires. Wildfires with small extension have been observed following major explosions [Rosi *et al.*, 2013], whereas large-scale wildfires can be triggered either by paroxysms [Giordano and de Astis, 2020; Turchi et *al.* 2020] or human activities.

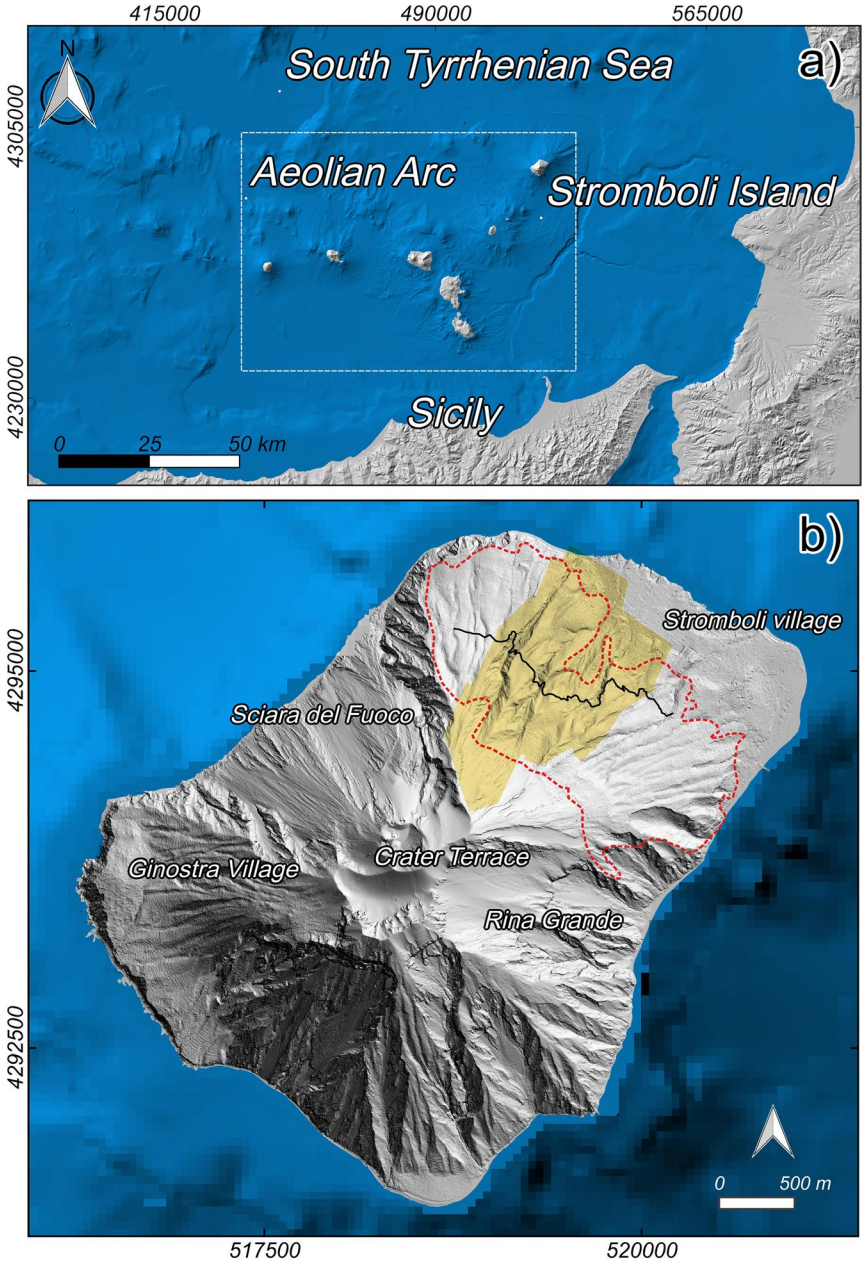

Figure 1. Geographical setting of Stromboli Island (WGS84 UTM33). The red dotted line roughly represents the area burned by the 24-25 May 2022 wildfire. The yellow area represents the area covered by the UAS March 2023 survey of this work. In black, we show the scenic trail as it was in the 2012.

On 25-26 May 2022, Stromboli was affected by large wildfire, caused by human activity that destroyed hectares of dense Mediterranean bush and vegetation that covered its NE flank. On 12 August 2022, heavy rainfall hit the island and remobilized a large amount of incoherent deposits that formed debris flows and flooded the houses and the roads downstream to the burnt areas. Following the 12 August 2022 event, other, minor, flooding events occurred at least on 13 October 2022, 5 November 2022 and 6 December 2023, 15 May 2023.

In late-March 2023, just before the large spring vegetation growth, we conducted an extensive Unmanned Aerial System (UAS) photogrammetric campaign over a portion of the NE flank of Stromboli Island that was heavily affected by the May 2022 wildfire first and by the debris flows later (Fig. 1). During the UAS campaign, we acquired 5922 photographs during 28 surveys for a total area covered of about 1.4 km^2 (Fig. 2). The photographs acquired were used to generate the Digital Surface Model (DSM) and the orthomosaic of the area through Structure from Motion (SfM) and Multi-view Stereo Matching (MSM) methods [Favalli *et al.*, 2012, 2018; James *et al.*, 2020].

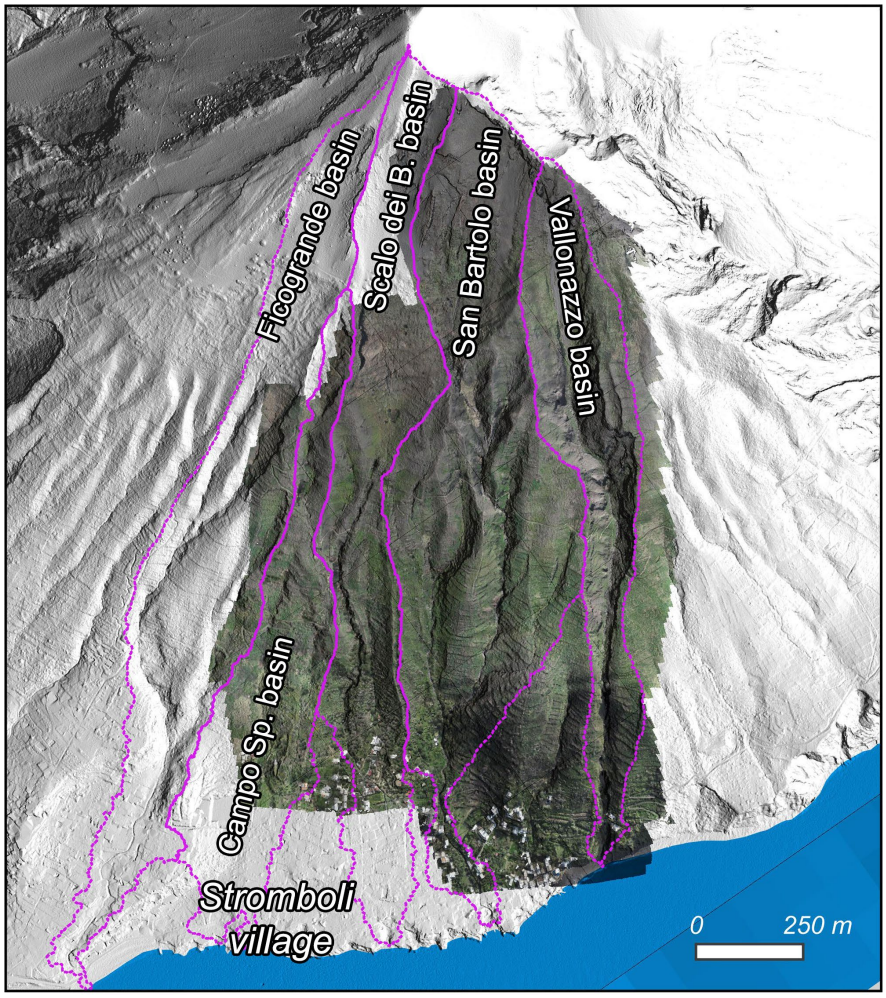

Figure 2. Hillshading of the NE flank of the Stromboli Island draped by the mosaic of the orthophotos generated from the UAS-acquired images. The purple dotted lines represent the Vallonazzo basin, the San Bartolo basin, the Scalo dei Balordi basin, the Campo Sportivo basin and the Ficogrande basin.

In this work, we present and share with the scientific community and local authorities the 10 cm resolution DSM and its derivative maps and the 1.6 cm resolution orthomosaic. These data show the consequences of the May 2022 wildfire and the following debris flows over a large area of the NE flank of the volcano. By comparing the 2023 DSM here generated and the 1 m-resolution 2012 LiDAR Digital Elevation Model (DEM), we also created the corresponding elevation difference map that provides preliminary overview of the amount of the deposits removed from the NE flank.

2. Geological context

The island of Stromboli is the 924 m-high emerged portion of a ~3000 m-high active stratovolcano located in the Tyrrhenian Sea, off the southern coast of Italy (Figure 1). It is in a perennial state of activity characterized by persistent, ordinary explosive activity of low-intensity events occurring about every 10-20 minutes, punctuated by occasional, sudden, more violent explosions. Violent explosions range from small-scale paroxysms, also called "major explosions" [Batberi *et al.*, 1993], to large-scale "paroxysms" [Bertagnini *et al.*, 2011; Bevilacqua *et al.*, 2020].

The morphology of Stromboli is shaped by two large scars resulting from several large mass-wasting phenomena: i) the Sciara del Fuoco on the NW flank, a large and unstable scar where most of the eruptive products now ends; and ii) Rina Grande on the SE flank [Tibaldi *et al.*, 2001; Romagnoli *et al.* 2009; Di Roberto *et al.*, 2010].

The 2023 UAS surveys acquired a vast area of the NE sector of the Island largely interested first by the wildfire of May 2022 (Figure 1) and later by the August 2022 debris flows. Five hydrological basins are captured during the surveys: four of them entirely or almost entirely, and one only partially (Figure 2). The basins are named according to their discharge locations on the coastline, i.e. from the NW to SE, Vallonazzo basin, San Bartolo basin, Scalo dei Balordi basin, Campo Sportivo basin and Ficogrande basin (Figure 2). This area is characterized by medium to gentle slopes, largely less than 30° [Fornaciai *et al.*, 2010]. It is a heterogeneous area in which epiclastic and reworked deposits belonging to the recent, neo- and palaeo-activity of the volcano accumulated naturally [Apuani *et al.*, 2005].

The field activities made us face the dramatic consequences of the 2022 wildfire and debris flows. The village was cleaned soon after the main event of August 2022, but the NE flank of the volcano in March 2023 still showed numerous recently carved channels where the maximum observed thickness of removed deposits exceeding 2 meters (Figure 3).

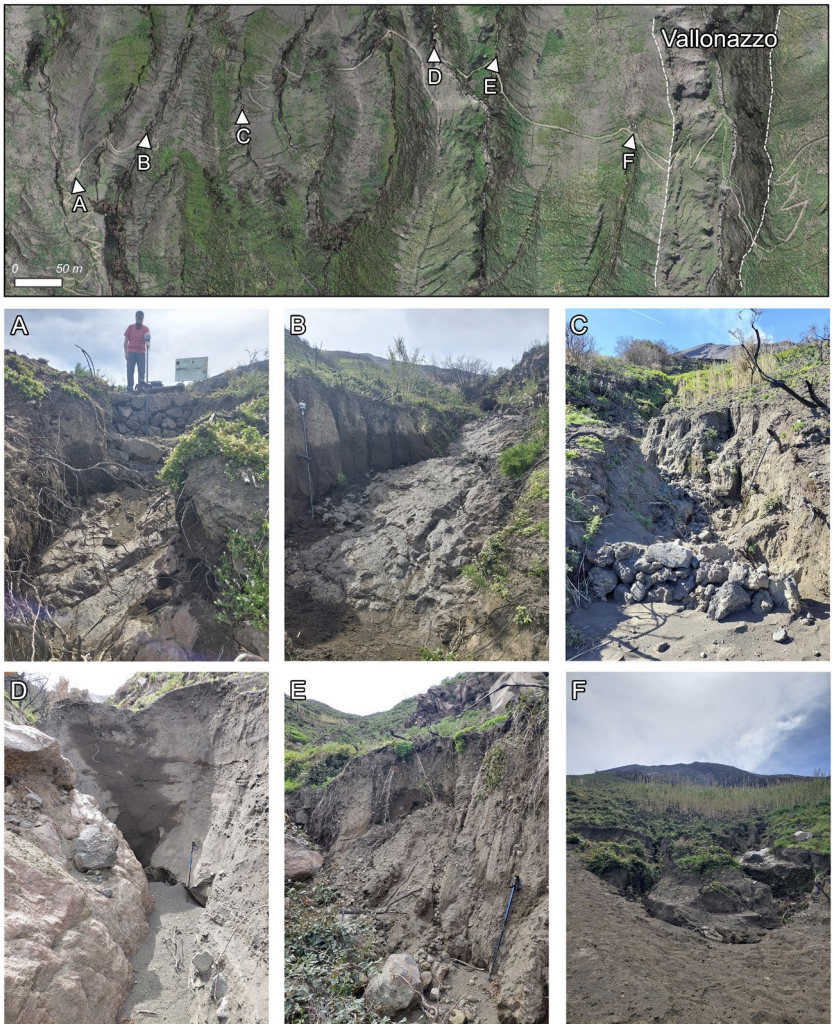

Figure 3. Photographs taken along the scenic trail showing some of the channels carved by the 12 August 2022 rainstorm and the following events. The triangles indicate the location of the shooting points.

3. UAS surveys and data generation

In late March 2023, an extensive UAS survey was carried out on the NE flank of Stromboli volcano over an area heavily affected by the remobilization of incoherent deposits due to the 12 August 2022 rainfall and the following events (Figures 2 and 3). The campaign was conducted using technologies and expertise supplied by the Istituto Nazionale di Geofisica e Vulcanologia, Sezione di Pisa, Laboratorio di Modellistica 3D. The survey was carried out by two UASs: a DJI Phantom Pro and a DJI Phantom Pro real-time kinematic (RTK). UAS surveys were supported by a simultaneous GPS campaign made by a R10 Trimble RTK Differential GPS (DGPS) used to acquire a set of points on the ground. 28 UAS surveys were carried out. The mean flight elevation was 62.7 m above ground level. A total of 5922 photographs were acquired. The surveys covered an area of 1.4 km^2 that included most of the Vallonazzo, San Bartolo and Scalo dei Balordi basins (Figures 2 and 3). The photographs acquired during the UAS surveys were used to generate the DSMs and the orthomosaic (Figure 4) of the area through Structure from Motion (SfM) and Multi-view Stereo Matching (MSM) methods [Favalli *et al.*, 2012, 2018; James *et al.*, 2020]. We processed the photos using the Agisoft Metashape Professional version 1.6.2. software, which implements the SfM and the MSM algorithms.

We also generated morphometric variables useful for the geomorphological mapping, i.e. the shaded relief map, the slope map, the sky view factor (SVF) map [Steyn, 1980; Zakšek *et al.*, 2011], and the openness down [Yokoyama *et al.*, 2002] map (Figure 5). The SVF variable is defined in terms of the solid angle (Ω) open to the sky and it is expressed as the sky percentage visible from any given point of the surface, i.e., $SVF = \Omega/2\pi$ [Favalli and Fornaciai, 2017]. Since ridges, lines and crests will be incident to nearly all of the incoming light, as consequence these features will have SVF values close to one. The opposite will be for depressed areas. Openness down is the measure of the belowground openness [Yokoyama *et al.*, 2002]. It has high values inside valleys, gullies, thalwegs, fractures and so on [Favalli and Fornaciai, 2017].

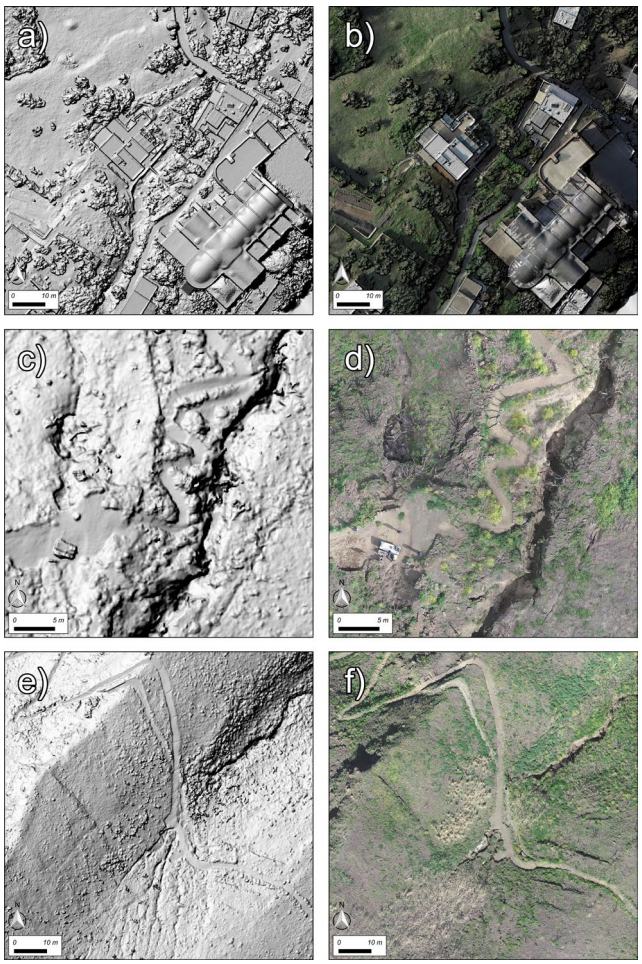

Figure 4. Details of hillshaded DSM and orthophotos at different scales. a) and b) The San Bartolo church. c) and d) The panoramic point at 290 m a.s.l. along the path. e) and f) The panoramic trail before the Vallonazzo valley.

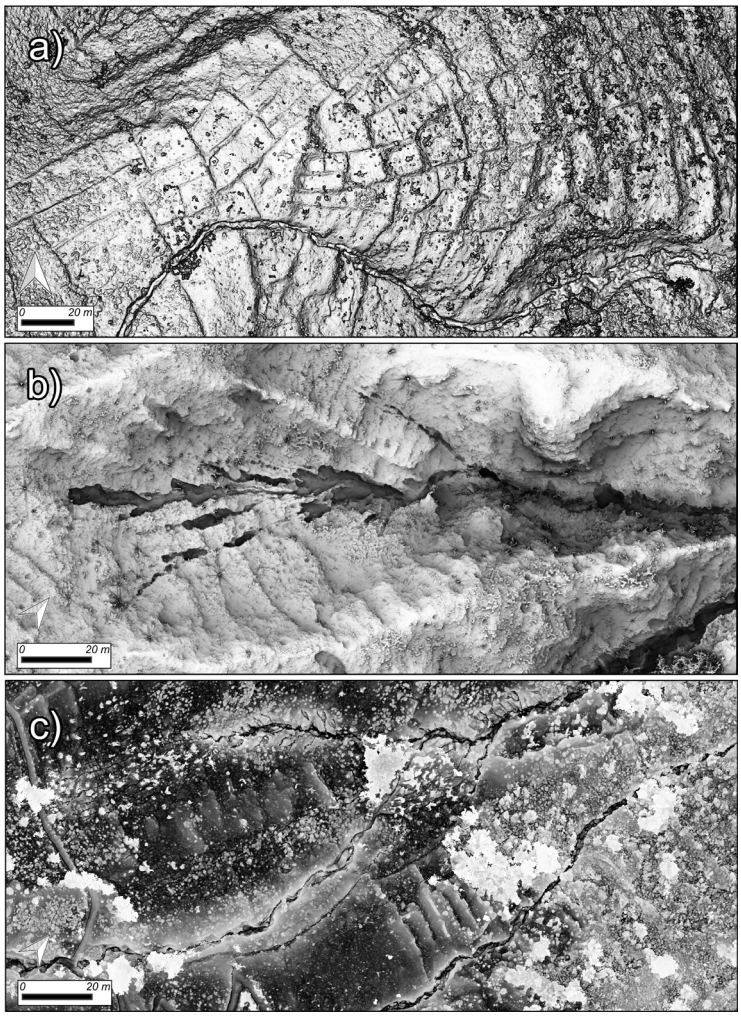

Figure 5. DSM-derivated variables maps of three different areas: a) Slope map showing a terraced area just above the village; b) Sky View Factor map showing an uppermost area of detachment recently carved; and c) Openness down map showing a conjunction point between two channels. The scattered white areas are the trees and bushed survived to the wildfire.

4. Results

The resulting 3D point cloud had a ground resolution of 1.69 cm/pixels. The initial 3D model was generated using the collected photos, the ground control points provided by the system RTK Base Station and Rover, in our case the DJI Phantom Pro 4 RTK. The model was then accurately georeferenced using the coordinates of the 106 GPS points taken on the ground and, in addition, the coordinates of a few recognizable (anchor) points on the uppermost sector of the imaged area extracted from a pre-existing 2012 LiDAR-DEM. This last data was necessary because the 3D model was generated using data acquired by UASs both with and without RTK. In particular, the uppermost area was imaged by the no-RTK UAS and without the above-mentioned anchor points, the 3D model would have had high errors in its upper edge. After the 3D reconstruction, the model had the following residual error: $XY_{error} = 3.65$ cm, $Z_{error} = 3.32$ cm, and total error = 4.94 cm.

The 3D model had a ground resolution of 1.69 cm/pixels, from which a DSM with resolution of 3.24 cm/pixel and mean point density of 955 points/m² was generated. The final data we produced consisted in a 10 cm high resolution DSM and in a 1.6 cm resolution orthomosaic of the imaged area (Figs. 2 and 4). We decided to generate a DSM at a lower resolution compared to the resolution suggested by the software to reduce the autocorrelation among neighbor pixels.

321 independent (i.e. not used for the georeferencing procedure) GPSs points, with XY mean error of 2.4 cm and Z mean error of 4.6 cm, were acquired to assess the 2023 DSM accuracy. By comparing with these data we calculated

the mean error, the median error and the root mean square error (RMSE) of the 2023 DSM. Figure 6 shows the vertical discrepancies of the 2023 DSM with respect to the 321 GPSs points as a histogram of the discrepancies [Höhle and Höhle, 2009]. The histogram shows that the error has a normal distribution. To compare it with a normal distribution, we also plotted a curve of a normal distribution (total Gaussian distribution) and a curve of a normal distribution truncated at the 3s threshold. In addition, we calculated the normalized median absolute deviation (NMAD), which is less sensitive to the presence of outliers [Höhle and Höhle, 2009]. All the metrics parameters reported in Figure 6 are in meters.

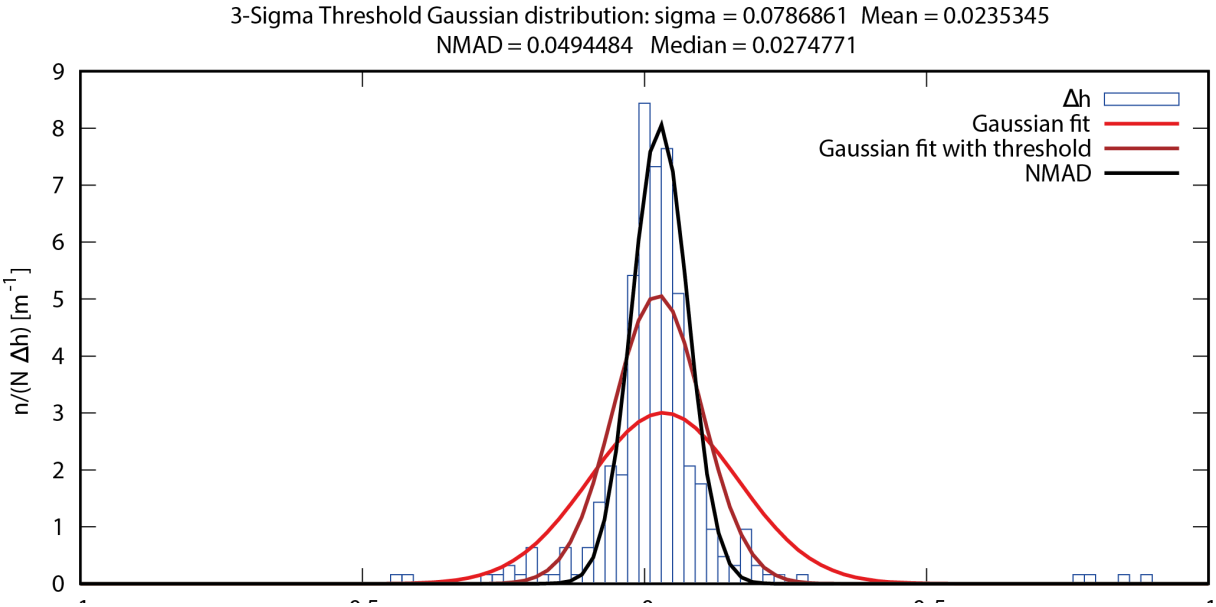

Figure 6. Histogram of the differences Δh between the 2023 DSM and the 321 GPSs points in meters in the range [−1 m, 1 m]. Superimposed on the histogram are reported the corresponding normal distribution curves and the NMAD distribution.

The UAS-derived DSM was compared with the 2012 1 m-resolution Digital Elevation Model (DEM), obtained from an airborne LiDAR survey, by creating a map of the topographic differences between 2023 and 2012 (Figure 7). The 2012 Airborne LiDAR survey preceded by about 10 years the disastrous events of 2022, but there were no other significant comparable land waste phenomena in that period, on the NE slopes. The 2012 LiDAR-DEM was obtained from data acquired during an airborne survey carried out by "BLOM Compagnia Generale Riprese aeree S.P.A." (www.blomasa.com). The topographic data were acquired using the Leica ADS80 sensor, which has instrumental vertical and horizontal accuracy of $\pm$ 10/20 cm and $\pm$ 25 cm, respectively. The acquired point cloud had a mean point density of 8 pt/m^2 [Di Traglia *et al.*, 2020]. During the 2012 LiDAR survey, also an orthophoto with resolution of 20 cm was acquired.

The 2023-2012 data difference was used both to detect the topographic changes due to natural phenomena and for model-to-model accuracy assessment. Conversely to using GPS points for accuracy assessment, this difference has the advantage of fully representing the terrain details [Wessel *et al.*, 2018]. DEM of difference is typically affected by errors depending on mismatches between two DEMs of the same area, which leads to artifacts in the elevation differences [Favalli *et al.*, 2010] that are visible in the areas that should not have been affected by relevant natural changes. The differences map, calculated by differencing cell-by-cell the height values, showed a good matching between the 2023 DSM and the 2012 LiDAR DEM (Figure 7). Although most of the vegetation was burned at the time of the survey, we must keep in mind that the 2023 data is a DSM and, as a consequence, the height measurement includes trees, buildings and other above-ground structures. These are clearly visible in Figure 7 where the above-ground structures (not present in the 2012 DEM) have been depicted as added features. Besides these features, Figure 7 shows minimal discrepancies between the two data in the village (streets and buildings planimetry, Figure 7b) and along the scenic trail (Figure 7c).

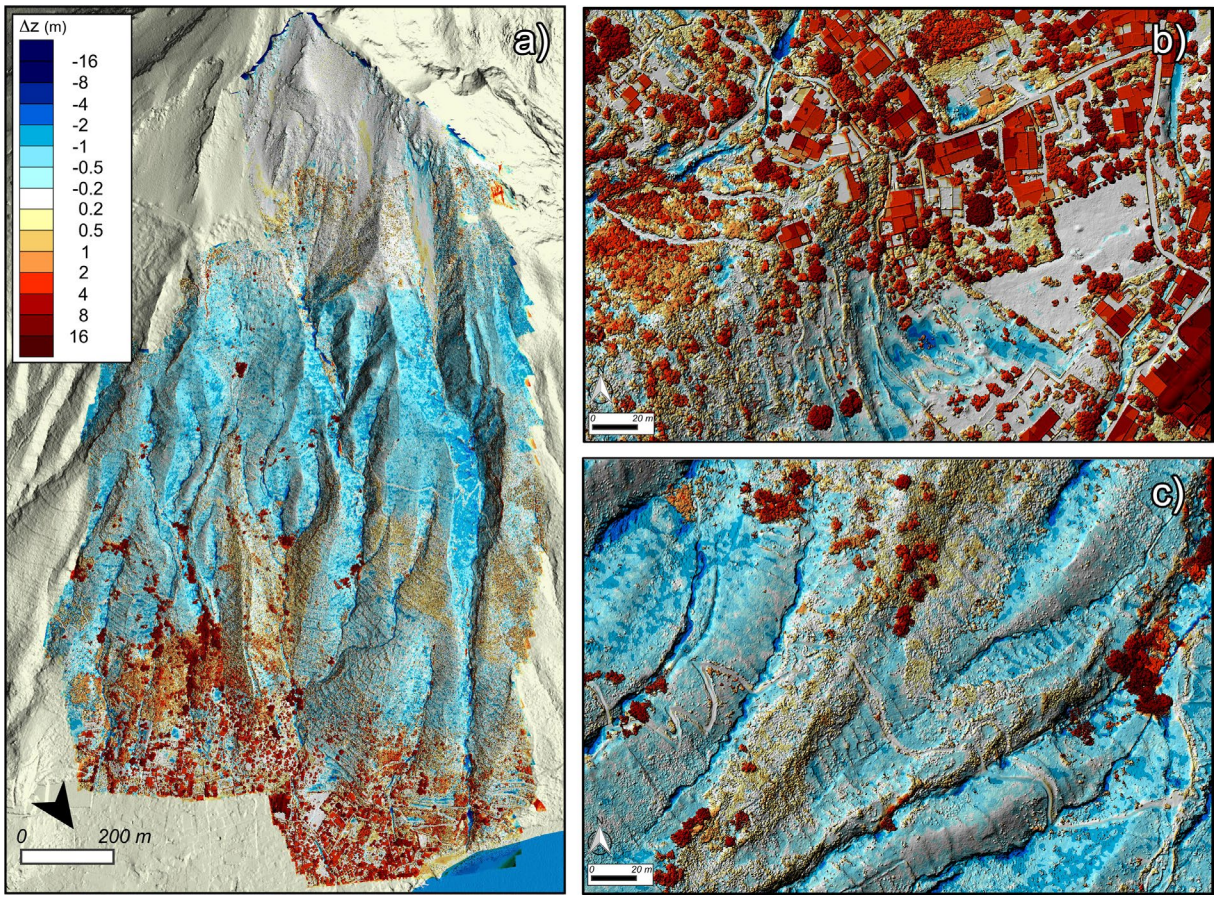

Figure 7. 2023-2012 topographic difference. a) The difference over the whole acquired area shows the distribution of the elevation differences in meters. In light yellow the 2012 hillshaded DEM. b) Detail of the village shows the good *x*, *y* and *z* matching between the 2012 and 2023 datasets. c) Detail of the flank that shows a general decrease of *z* from 2012 to 2023 over the vegetated area except above the San Bartolo lava flow. The scenic trail shows a good match between the two DEMs.

The data set we share consists of: i) high-resolution (0.1 m/pixel) Digital Surface Model; ii) high-resolution (0.016 m/pixel) orthomosaic divided in 23 tiles; iii) DSM derived maps, i.e. the Hillshaded (azimuth = 315 m elevation = 45°) map, the Sky View Factor map and the openness down map. The DSM and the orthomosaic were generated by processing UAS photographs using Agisoft Metashape®. Details of the photogrammetric survey data and elaboration are described above. The UAS derivated maps are generated using a C++ code developed *ad-hoc* [Favalli and Fornaciai 2017]. All data are in WGS84 UTM 33N Coordinate System and provided in GEOTIFF file format. The dataset is stored in the Istituto Nazionale di Geofisica e Vulcanologia (INGV) repository under CC BY 4.0 use license.

5. Discussion and Conclusion

After the 25-26 May 2022 wildfire, the 12 August 2022 heavy rain, and the following events, left on the NE flank of Stromboli Island numerous deep furrows. Walking along the scenic trail, the dramatic consequences of these events were evident (Figure 3). All visible flow paths were affected by mass wasting. In some of them, the deposit wasting led to the outcropping of the underlying lava flows (Figures 3a and b), in others, the thicknesses of removed deposits exceeded the 2 meters (Figures 3b, d and e). With the purpose of having a more clear and synoptic picture of the gullies reactivation and regeneration on the NE flank, a UAS campaign was carried out in late March 2023. The campaign was held in March and at the lowest possible flight altitude with the aim of imaging also the smaller signs of erosion in the inaccessible areas before they were covered again by the vegetation. Moreover, we planned

the starting and landing points of all our flights at reasonable low elevation taking into account both the national flight regulation and the risk to be affected by ballistic fall of major explosions and paroxysms [Barberi *et al.*, 1993; Rosi *et al.*, 2013].

The area under study was selected because it was affected by the deposit-derived pyroclastic density currents following the paroxysm of 11 September 1930 [Rittmann, 1931; Di Roberto *et al.*, 2014]. In fact, the burnt vegetation and the following erosion prompted a field survey, performed at the same time of our UAS survey, to retrieve the pyroclastic flow deposits in the lower portion of San Bartolo basin that are described by some of the historical sources [Abbruzzese, 1936].

The DSM and orthomosaic that we generated from the photographs taken during the March 2023 campaign covers about one-third of the area affected by the May 2022 wildfire (Figure 3). The area was the source of several debris flows that flooded the village of Stromboli in August 2022 and later. In particular, the 1.6 cm resolution orthomosaic shows with great details the stream network and the areas of deposit detachment (Figure 8). Even though the presence of both newborn and residual vegetation somehow disturbs the topographic data in the DSM, the 10 cm DSM can be used to measure preliminarily the thickness of deposits lost inside the channels (Figure 8).

Taking into account that the map of difference in Figure 7 is obtained by subtracting a DEM (the surface of the terrain) from a DSM (i.e., the surface of any object on the ground, including vegetation, building, etc), we observe a general decrease in elevation from 2012 to 2023 in the investigated area (Figure 7a). This general trend presents some patches where the elevation, conversely, increases, especially along the Lava di San Bartolo (Figure 7). Considering that village streets, squares and the building perimeters, as well as the scenic trail, present a good matching between the 2012 DEM and 2023 DSM (average difference less than 20 cm), we did not apply further co-registrations. We exclude that the observed general z decrease was due to either systematic errors in the original data or to the difference in the acquisition methods. We hypothesize that it is mainly ascribed to the loss of the vegetation cover due to the wildfire. In fact, although the 2012 LiDAR DEM was cleaned from the vegetation, we cannot know how effective the removal of vegetation from the 2012 data has been. Fornaciai *et al.* [2010] described how the complete vegetation removal from LiDAR raw data at Stromboli could be difficult and often impossible.

Moreover, the resolutions of the 2012 and 2023 data sets differ by one order of magnitude. Some features that are detectable in the 0.1 m resolution dataset could not have been imaged in the 1 m resolution dataset, which means that they will appear as volume addition or removal. For example small gullies (e.g. less than 1 m) not viewed by the 2012 DEM, will instead be present in the 2023 DSM. As a consequence, the difference of DEMs will show this bias as a new carved channel. This prevented us from calculating the volume of removed material from 2012 to 2023. The gullies areas were too small, and the residual displacement between the two datasets was too high; therefore, the error in the calculated volume would have been too significant. Despite that, the analysis of the data set and the profiles pre- and post- events give us information on the dynamics of the 2022 debris flows and allow us to extract useful data.

The 2012 orthophoto shows that all the gullies detectable in the 2023 orthomosaic were covered by vegetation (Figure 8). Profiles 1, 2, and 5 of Figure 8 show that the thickness of deposits lost may exceed 4 meters. Profile 3 represents two channels, both of which were carved up to reach the lava flows at the bottom. Profile 4, which is located near Figure 3d, illustrates the dynamic of a large channel that was partially empty in 2012, between 2012 and 2023 it was filled by reworked deposits and, finally, the August 2022 rainfall and the following events had it carved partially. Profiles 5 and 6 represent the uppermost source area of two different flows. In the former, there is one single large area carved, in the latter there is a more complex system of channels.

The data set that we produced and shared represents with great accuracy a large area of the NE sector of Stromboli Island that generated the debris flow that hit the village in August 2022. It allows identifying the source areas and extracting 3D data about the relative gullies. In addition, it is possible to observe possible areas of weakness and prone to the future detachment before they will be covered again by the vegetation.

It would be useful to extend the area of the survey and compare this data set with pre-event DEMs at higher resolution in order to calculate the volume of removed deposits.

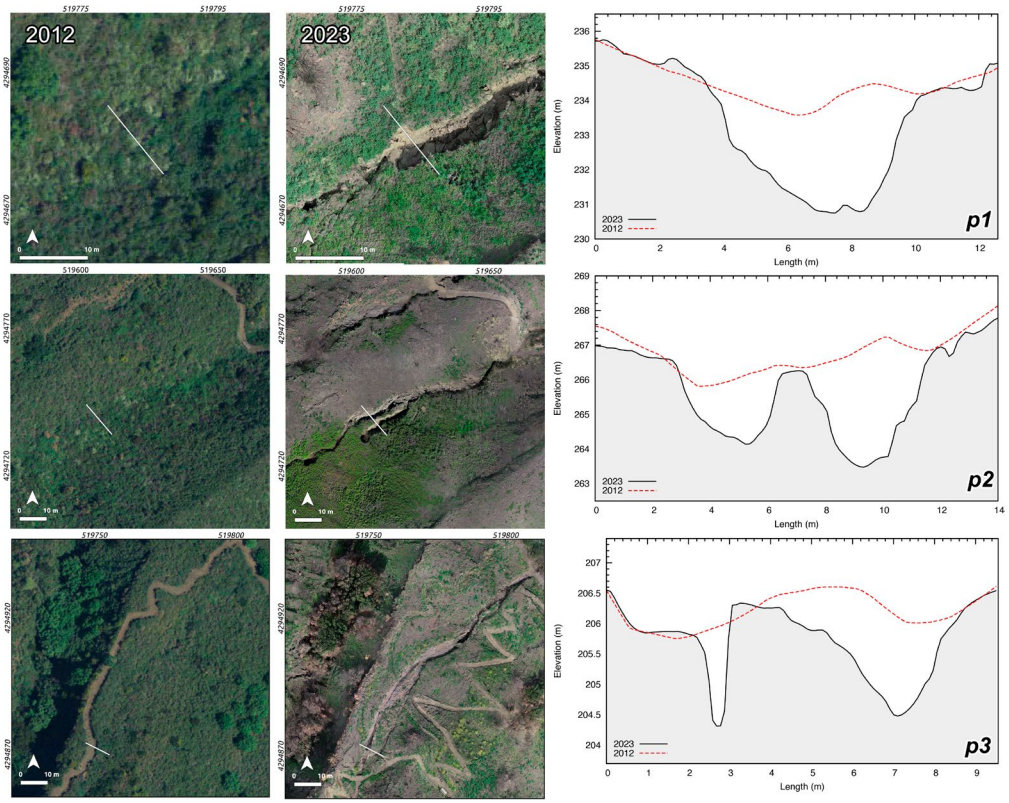

Figure 8. Part 1. Selected profiles extracted from the 2012 DEM and the 2023 DSM. Frames of the 2012 photo acquired during the LiDAR survey and of the 2023 orthomosaic (WGS84 UTM33 Coordinate Reference System) are also shown to highlight the topographic and vegetation changes as well as the location of the profiles.

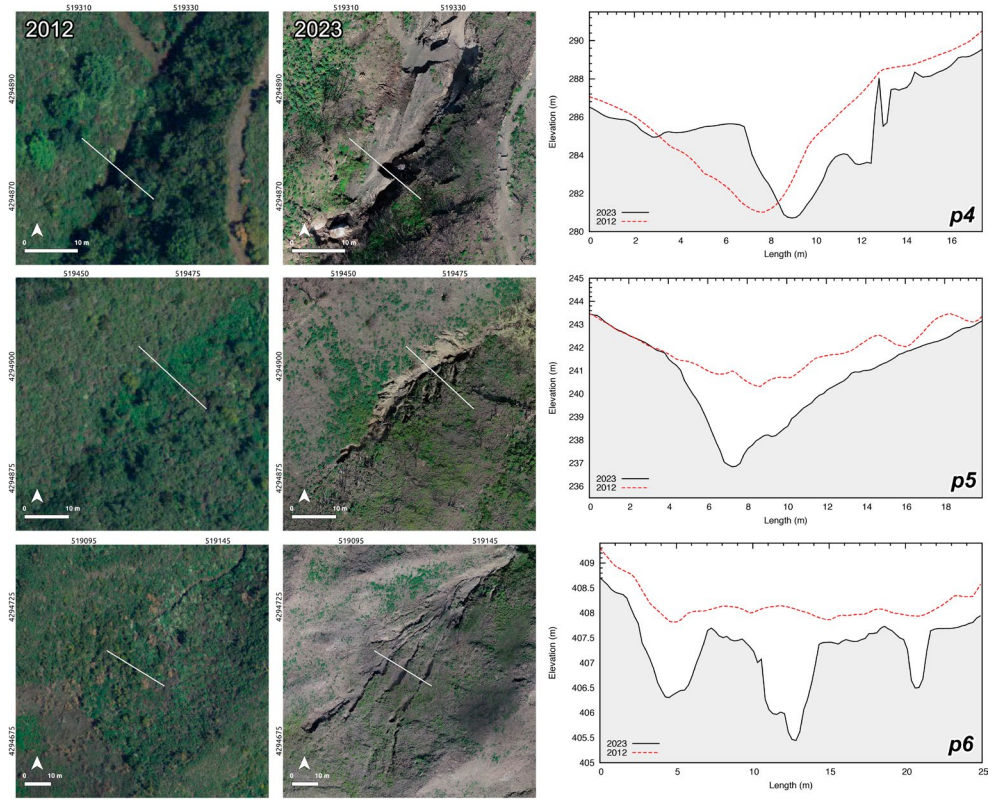

Figure 8. Part 2. Selected profiles extracted from the 2012 DEM and the 2023 DSM. The 2012 and 2023 orthophotos are also shown.

Data Availability Statement. The data generated in this study are stored in the Istituto Nazionale di Geofisica e Vulcanologia, Sezione di Pisa repository (https://doi.org/10.13127/stromboli/2023-uas-survey) and are shared under CC BY 4.0 use license.

Acknowledgement. This research is supported by Agreement DPC – INGV All. B, 2022-2024 – "Sistema Unico Stromboli, Task 4.1: Elements for risk assessment of ballistic projectiles, pyroclastic avalanches and tsunamis at Stromboli", and by project "Reti multiparametriche – Sotto-progetto Vulcani", INGV, 2022-2025. Objective A7: "Probability of eruptive fenomena and hazard maps of ballistics and secondary pyroclastic flows from major explosions and paroxysms with risk assessment implications".

References

Abbruzzese, D (1936). Sulla catastrofica esplosione dello Stromboli dell'11 settembre del 1930, Atti Accad. Gioenia Sc. Nat. Catania 1, 1-33.

Apuani, T., C. Corazzato, A. Cancelli and A. Tibaldi (2005). Physical and mechanical properties of rock masses at Stromboli: a dataset for volcano instability evaluation, Bull. Engin. Geol. Environ., 64, 419-431.

Areu-Rangel, O.S., R. Bonasia, F. Di Traglia, M. Del Soldato and N. Casagli (2020). Flood susceptibility and sediment transport analysis of Stromboli Island after the 3 July 2019 paroxysmal explosion, Sustainability, 12, 8, 3268.

Barberi, F., M. Rosi, and A. Sodi (1993). Volcanic hazard assessment at Stromboli based on review of historical data, Acta Vulcanol., 3, 173-187.

Bertagnini, A., A. Di Roberto and M. Pompilio (2011). Paroxysmal activity at Stromboli: lessons from the past, Bull. Volcanol., 73, 9, 1229-1243

Bevilacqua, A., A. Bertagnini, M. Pompilio, P. Landi, P. Del Carlo, A. Di Roberto, W. Aspinall and A. Neri (2020). Major explosions and paroxysms at Stromboli (Italy): A new historical catalog and temporal models of occurrence with uncertainty quantification, Scientific reports, 10(1), 17357.

Bisson, M., M. Favalli, A. Fornaciai, F. Mazzarini, I. Isola, G. Zanchetta and M.T. Pareschi (2005). A rapid method to assess fire-related debris flow hazard in the Mediterranean region: An example from Sicily (southern Italy), Int. J. Appl. Earth Obsserv. Geoinfo., 7, 3, 217-231.

Di Roberto, A., M. Rosi, A. Bertagnini, M.P. Marani and F. Gamberi (2010). Distal turbidites and tsunamigenic landslides of Stromboli volcano (Aeolian Islands, Italy), In Submarine Mass Movements and Their Consequences; Springer: Dordrecht, The Netherlands, 719-731.

Di Roberto, A., A. Bertagnini, M. Pompilio and M. Bisson (2014). Pyroclastic density currents at Stromboli volcano (Aeolian Islands, Italy): A case study of the 1930 eruption, Bull. Volcanol, 76, 827.

Di Traglia, F.A. Fornaciai, M. Favalli, T. Nolesini and N. Casagli (2020). Catching Geomorphological Response to Volcanic Activity on Steep Slope Volcanoes Using Multi-Platform Remote Sensing, Remote Sens., 12, 438.

Favalli, M., A. Fornaciai, F. Mazzarini, A. Harris, M. Neri, B. Behncke, M.T. Pareschi, S. Tarquini and E. Boschi (2010). Evolution of an active lava flow field using a multitemporal LIDAR acquisition, J. Geophys. Res., Solid Earth, 115, B11.

Favalli, M., A. Fornaciai, I. Isola, S. Tarquini and L. Nannipieri (2012). Multiview 3D reconstruction in geosciences, Compu. Geosci., 44, 168-176.

Favalli, M. and A. Fornaciai (2017). Visualization and comparison of DEM-derived parameters. Application to volcanic areas, Geomorphology, 290, 69-84.

Favalli, M., A. Fornaciai, L. Nannipieri, A. Harris, S. Calvari and C. Lormand (2018). UAV-based remote sensing surveys of lava flow fields: a case study from Etna's 1974 channel-fed lava flows, Bull. Volcanol., 80, 3, 1-18.

Fornaciai, A., M. Bisson, P. Landi, F. Mazzarini and M.T. Pareschi (2010). A LiDAR survey of Stromboli volcano (Italy): Digital elevation model-based geomorphology and intensity analysis, Int. J. Remote Sens., 31(12), 3177-3194.

Giordano, G. and G. De Astis (2021). The summer 2019 basaltic Vulcanian eruptions (paroxysms) of Stromboli, Bull. Volcanol., 83, 1.

Giovannini, G. (1994). The effect of fire on soil quality. Soil erosion as a consequence of forest fires, Geoforma Ediciones, Logroño, 15-27.

Giovannini, G., R. Vallejo, S. Lucchesi, S. Bautista, S. Ciompi and J. Llovet (2001). Effects of land use and eventual fire on soil erodibility in dry Mediterranean conditions, Forest Ecology and Management, 147, 1, 15-23.

Höhle, J. and M. Höhle (2009). Accuracy assessment of digital elevation models by means of robust statistical methods, ISPRS Journal of Photogrammetry and Remote Sensing, 64, 4, 398-406.

https://www.ct.ingv.it/index.php/formazione-e-divulgazione/news/328-l-alluvione-di-stromboli-del-12-agosto-2022.

James, M.R., B. Carr, F. D'Arcy, A. Diefenbach, H. Dietterich, A. Fornaciai, E. Lev, E.J. Liu, D.C. Pieri, M. Rodgers, B. Smets, A. Terada, F.W. von Aulock, T.R. Walter, KT. Wood and E. Zorn (2020). Volcanological applications of unoccupied aircraft systems (UAS): Developments, strategies, and future challenges, Volcanica, 3, 1, 67-114.

Ortíz-Rodríguez, A.J., C. Muñoz-Robles and L. Borselli (2019). Changes in connectivity and hydrological efficiency following wildland fires in Sierra Madre Oriental, Mexico, Sci. Total Environ., 655, 112-128.

Providoli, I., H. Elsenbeer and M. Conedera (2002). Post-fire management and splash erosion in a chestnut coppice in southern Switzerland, Forest ecology and management, 162, 2-3, 219-229.

Rittmann, A.D. (1931). Ausbruch des Stromboli am 11 September 1930, Zeits. Vulkanol., 14, 47-77.

Romagnoli, C., P. Kokelaar, D. Casalbore, F.L. Chiocci (2009). Lateral collapses and active sedimentary processes on the northwestern flank of Stromboli volcano, Italy. Mar. Geol., 265, 101-119.

Rosi, M., M. Pistolesi, A. Bertagnini, P. Landi, M. Pompilio and A. Di Roberto (2013). Chapter 14 Stromboli volcano, Aeolian Islands (Italy): present eruptive activity and hazards, Geological Society, London, Memoirs, 37, 1, 473-490.

Tibaldi, A. (2001). Multiple sector collapses at Stromboli volcano, Italy: How they work, Bull. Volcanol., 63, 112-125.

Thouret, J.C., S. Antoine, C. Magill and C. Ollier (2020). Lahars and debris flows: Characteristics and impacts, Earth-Sci. Rev., 201, 103003.

Turchi, A., F. Di Traglia, T. Luti, D. Olori, I. Zetti and R. Fanti (2020). Environmental aftermath of the 2019 Stromboli eruption, Remote Sens., 12(6), 994.

Turchi, A., F. Di Traglia, R. Gentile, A. Fornaciai, I. Zetti and R. Fanti (2022). Relative seismic and tsunami risk assessment for Stromboli Island (Italy), Int. J. Disaster Risk Reduct., 76, 103002.

Wessel, B., M. Huber, C. Wohlfart, U. Marschalk, D. Kosmann and A. Roth (2018). Accuracy assessment of the global TanDEM-X Digital Elevation Model with GPS data, ISPRS J. Photogram. and Remote Sens., 139, 171-182.

Wondzell, S.M. and J.G. King (2003). Postfire erosional processes in the Pacific Northwest and Rocky Mountain regions, Forest Ecol. Manag., 178(1-2), 75-87.

Yokoyama, R., M. Shirasawa and R.J. Pike (2002). Visualizing topography by openness: A new application of image processing to digital elevation models, Photogram. Engin. Remote Sens., 68, 3, 257-266.

Zakšek, K., K. Oštir and Ž. Kokalj (2011). Sky-view factor as a relief visualization technique, Remote Sens., 3, 2, 398-415.

***CORRESPONDING AUTHOR: Alessandro FORNACIAI**

Istituto Nazionale di Geofisica e Vulcanologia, Pisa, Italy

e-mail: alessandro.fornaciai@ingv.it